Adaptive generalized periodic boundary conditions for lattice Boltzmann simulations of pressure-driven flows through confined repetitive geometries

Oliver Gräser[1,*] and Andrej Grimm[2,†]
[1]*Department of Physics, The Chinese University of Hong Kong, Shatin, Hong Kong, China*
[2]*Department of Physics, National University of Singapore, Singapore*
(Received 19 January 2010; revised manuscript received 22 April 2010; published 13 July 2010)

An algorithm for an adaptive boundary condition for the simulation of fully developed, pressure driven flows using the lattice-Boltzmann method is introduced. The method simulates the effect of the solid walls confining a structure with dual periodicity, such as used in microfluidic devices. We combine a recently introduced boundary condition by Kim and Pitsch [Phys. Fluids **19**, 108101 (2007)] for the treatment of pressure driven flows in periodic structures with a controller loop that adjusts a perpendicular pressure gradient to suppress any net momentum perpendicular to the outer walls. The method's accuracy in asymmetric geometries is tested against a periodic array structure that uses regularized zero-velocity boundary conditions as outer walls.

DOI: 10.1103/PhysRevE.82.016702 PACS number(s): 47.11.−j, 47.61.−k

I. INTRODUCTION

The lattice Boltzmann method (LBM) has become an increasingly popular tool for the simulation of hydrodynamic flows [1–3]. Within the simulated system, the state of the fluid at each lattice node is defined through distribution functions of particle populations of certain discrete velocities. The observables at each lattice node, namely, fluid velocity and density, are functions of these populations. Typically, the distribution function is not fully specified on the boundary nodes.

Various options exist for deriving estimates of the distribution function on the boundary nodes. Simple periodic boundary conditions are often used if surface effects may be neglected [2]. Solid walls may be simulated using a simple bounce-back mechanism [4]. In addition, various methods have been proposed to derive these populations if values for either pressure or velocity on the boundary are known [5–8].

If one wants to exploit spatial periodicity of a system, additional difficulties arise because the state of the flow in any unit cell depends on configurations, i.e., pressure or velocity profiles that are defined at very distant points only. A typical example is a flow through a duct with periodic obstacles, where a steady periodic flow pattern develops within a few unit cells [9]. In earlier works, the driving force—a pressure gradient over the entire duct—was often replaced by a body force akin to gravity [10]. Such a force alters the equilibrium distribution, and, hence, simple periodic boundary conditions (SPBC) may be used. This approach, however, requires a uniform cross-sectional area of the duct to give correct results. Recently introduced generalized periodic boundary conditions (GPBC) for periodic flow velocities [11] and momentum densities [12] with pressure gradients allow to simulate such geometries without having to resort to a body force.

In various systems, e.g., microfluidic devices [13–17], a pressure gradient generates a liquid flow through a two-dimensional repetitive array of identical unit cells that are confined by solid walls (see Fig. 1). Exploiting both periodicities of this system and therefore achieving greater accuracy is not yet possible with the previously proposed boundary conditions. For a system with two- or three-dimensional periodicity confined by solid walls, SPBC can only be used if the unit cell's geometry is symmetric with respect to the momentum transferred between fluid and obstacles. If SPBC are used in asymmetric unit cells (e.g., cells with a solid triangular obstacle), the flow will adjust its direction. Hence, a net flow component perpendicular to the pressure gradient will emerge in the fully developed state. In a real device, this

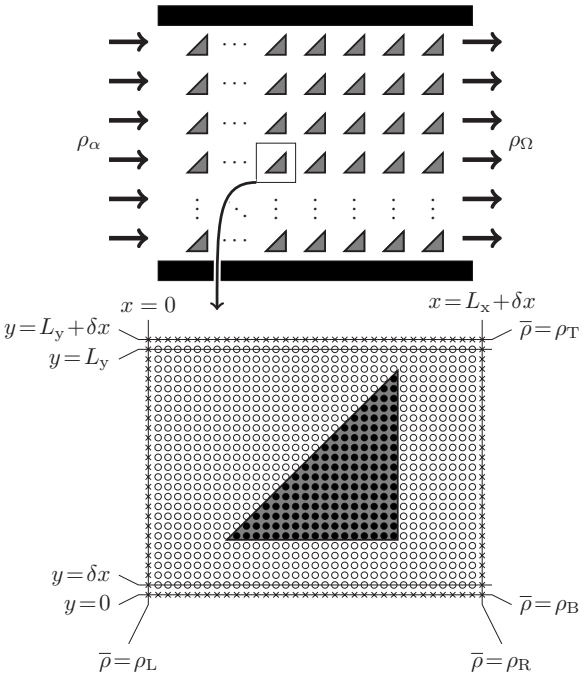

FIG. 1. Exemplary microfluidic device consisting of $M_x \times M_y$ unit cells. The layout of a single unit cell is magnified in the lower part. Symbols correspond to bounce-back dynamics (filled circles), BGK-dynamics (open circles), and boundary nodes (crosses). Overlined symbols $\overline{\rho}$ refer to averaging over the indicated row or column.

*graeser@phy.cuhk.edu.hk
†andrej.grimm@nus.edu.sg

perpendicular flow would be suppressed by the outer walls, which may lie many unit cell lengths outside the simulated cell. Any initial orthogonal flow will result in a pressure gradient until the forces resulting from obstacle and pressure gradient balance and the perpendicular component of the flow vanishes. In the present work, we describe a lattice Boltzmann method simulation setup that uses an adaptive perpendicular pressure gradient to suppress the perpendicular flow (see Sec. II). This second pressure gradient is adjusted through a standard proportional-differential (PD) controller loop, using the cell's vertical leakage and momentum as control variables. In Sec. III, simulation results for the proposed method and a reference system are presented and accuracy is discussed. A summary and outlook is given in Sec. IV.

II. METHODOLOGY

Within LBM, a set of Q lattice unit vectors $\mathbf{e}_i$; $i=0,\ldots,Q-1$ with lattice constant δx is defined—typically nine such vectors for a two-dimensional problem (D2Q9) and either 19 (D3Q19) or 27 (D3Q27) for a three dimensional problem. The state of the system is then described by a set of distribution functions $f_i(\mathbf{x},t)$ at every lattice node $\mathbf{x}$. These distributions correspond to the amount of molecules with a discrete velocity $\mathbf{u}_i=\mathbf{e}_i/\delta t$, δt being the time between two simulation steps [18]. The macroscopic parameters at a lattice node, i.e., the *density* ρ and *velocity* $\mathbf{u}$, can be calculated from these populations via

$$\rho=\sum_{i=0}^{Q-1} f_i; \quad \mathbf{u}=\sum_{i=0}^{Q-1}\frac{f_i\mathbf{e}_i}{\rho}. \tag{1}$$

The propagation or streaming of the system is given by

$$f_i(\mathbf{x}+\mathbf{e}_i,t+\delta t)-f_i(\mathbf{x},t)=\Omega(\mathbf{f})=-\frac{(f_i-f_i^{\mathrm{eq}})(\mathbf{x},t)}{\tau}. \tag{2}$$

The collision operator Ω is modeled according to the linear Bhatnagar-Gross-Krook (LBGK) relaxation operator [19] as a linear decay to the equilibrium. For a stable decay, the relaxation time has to be set to $\tau>0.5$. In addition, confining the relaxation time to $\tau<1$ has been found to minimize simulation errors [20,21]. The equilibrium distribution is defined as a quadratic expansion of the Maxwell-Boltzmann equilibrium distribution

$$f_i^{\mathrm{eq}}(\rho,\mathbf{u})=w_i\rho\left(1+\frac{\mathbf{e}_i\cdot\mathbf{u}}{c_s^2}+\frac{1}{2}\frac{(\mathbf{u}\cdot\mathbf{e}_i)^2}{c_s^4}-\frac{1}{2}\frac{u^2}{c_s^2}\right), \tag{3}$$

where the w_i are weight factors that depend on the chosen set of unit vectors and c_s is the speed of sound, which is set to $c_s=1/\sqrt{3}$. The equation of state $p=c_s^2\rho$ relates density and pressure. Our discussions will be based on a D2Q9-system of unit vectors. Extension to other systems, however, is straightforward.

An exemplary layout of a microfluidic device is shown in Fig. 1. A periodic grid of unit cells, each of size $L_x=N_x\delta x$, $L_y=N_y\delta x$, is confined by solid, no-slip outer walls and connected to reservoirs of different pressures ρ_α and $\rho_\Omega<\rho_\alpha$. The pressure difference over the system results in a periodic pressure gradient over each cell:

$$\rho(x,y)-\rho(x+L_x,y)=\Delta\varrho_x, \tag{4}$$

while the current flowing through the device is periodic: $\mathbf{j}(x,y)=\mathbf{j}(x+L_x,y)$. In an asymmetric geometry, a pressure gradient in y direction $\rho(x,y)-\rho(x,y+L_y)=\Delta\varrho_y$ will arise over time. In the fully developed state, it will suppress any net flow through any horizontal cross section over the unit cell interval:

$$j_\perp(y)=\int_x^{x+L_x} j_y(x,y)dx\overset{!}{=}0. \tag{5}$$

The boundary conditions for such a system have to take the periodicity of the momentum field in x and y direction into account. Furthermore, a constant pressure gradient in x direction driving the flow has to be maintained, while another pressure gradient in y-direction has to be applied to ensure $j_\perp=0$ in the fully established state.

For the boundary conditions in x direction we use GPBC that were suggested by Kim and Pitsch [12]. This approach combines periodic momentum density with a pressure gradient for one dimension. Fixed average densities are assumed on the right and left boundaries outside the unit cell: $\bar{\rho}(x=0)=\rho_L$ and $\bar{\rho}(x=L_x+\delta x)=\rho_R$. It should be noticed that the externally applied density difference $\Delta\rho_x=\rho_L-\rho_R$ is not identical to the periodic density gradient $\Delta\varrho_x$, since it is taken over a distance $L_x+\delta x$ slightly larger than the unit cell. Fluctuations in the pressure along the vertical boundaries are carried onward:

$$\rho(0,y)=\rho_L+\rho(L_x,y)-\bar{\rho}(L_x)$$

$$\rho(L_x+\delta x,y)=\rho_R+\rho(\delta x,y)-\bar{\rho}(\delta x). \tag{6}$$

The average densities on the inner boundaries, $\bar{\rho}(x=\delta x)$ and $\bar{\rho}(x=L_x)$, are not predefined but taken from the simulation. The velocity on the vertical boundaries, given these pressures and the periodicity condition, is

$$\mathbf{u}(0,y)=\frac{\rho(L_x,y)\mathbf{u}(L_x,y)}{\rho(0,y)}$$

$$\mathbf{u}(L_x+\delta x,y)=\frac{\rho(\delta x,y)\mathbf{u}(\delta x,y)}{\rho(L_x+\delta x,y)}. \tag{7}$$

The distribution functions on the corresponding nodes are given by the sum of the equilibrium distribution of the known density and velocity, and the nonequilibrium distribution of the corresponding periodic node:

$$f_i(0,y)=f_i^{\mathrm{eq}}[\rho(0,y),\mathbf{u}(0,y)]+f_i(L_x,y)-f_i^{\mathrm{eq}}(L_x,y)$$

$$f_i(L_x+\delta x,y)=f_i^{\mathrm{eq}}[\rho(L_x+\delta x,y),\mathbf{u}(L_x+\delta x,y)]+f_i(\delta x,y)-f_i^{\mathrm{eq}}(\delta x,y). \tag{8}$$

Additionally, we also use GPBC for the boundary conditions in y direction. As opposed to the x direction, the pressure gradient between the top and bottom boundary nodes $\Delta\rho_y=\rho_B-\rho_T$ is not constant, but is adjusted to suppress $j_\perp$. Densities, velocities and distributions on those boundary

nodes are defined analog to Eqs. (6)–(8). The density on the corner nodes is given through the periodicity conditions:

$$\rho(0,0) = \rho(L_x,L_y) + \Delta\varrho_x + \Delta\varrho_y$$

$$\rho(L_x + \delta x,0) = \rho(\delta x,L_y) - \Delta\varrho_x + \Delta\varrho_y$$

$$\rho(0,L_y + \delta x) = \rho(L_x,\delta x) + \Delta\varrho_x - \Delta\varrho_y$$

$$\rho(L_x + \delta x,L_y + \delta x) = \rho(\delta x,\delta x) - \Delta\varrho_x - \Delta\varrho_y. \quad (9)$$

Since $\Delta\varrho_x$ is not an a-priori known quantity, it has to be measured within the simulation, and the result will only be applicable in the fully developed state.

In the following, we introduce a controller algorithm to adapt ρ_B and ρ_T. In general terms, the average density on both boundaries needs to be adapted in order to suppress $j_\perp$. In a fully developed flow, Eq. (5) has to hold for any row y. However, $j_\perp$ for a single row is here not a suitable control variable. Especially during the initial phase, density fluctuations traveling through the liquid strongly affect $j_\perp$ when taken over a single row.

Alternatively, we can require the total perpendicular momentum of the fluid in the unit cell

$$j_y^{\mathrm{tot}} = \int_V j_y dx dy = \sum_{k=1}^{N_x}\sum_{l=1}^{N_y}\sum_{i=0}^{8} \mathbf{e}_y \cdot \mathbf{e}_i f_i(k\delta x, l\delta x) \quad (10)$$

to vanish. In this way, fluctuations even out when the integral is taken over the entire unit cell. Yet, the condition $j_y^{\mathrm{tot}}=0$ is not necessarily equivalent to Eq. (5): liquid might be flowing downward in the lower half of the cell and upward in the upper half such that Eq. (5) is not fulfilled for any single row. At the same time, the cell's total perpendicular momentum might vanish since the upward and downward momenta even out. To avoid this problem, we require the net leakage through the upper and lower boundary of the cell

$$\Phi_y = \oint_{\partial V} j_y \mathbf{e}_y d\mathbf{o}$$

$$= \sum_{k=1}^{N_x}\left[\sum_{i=2,5,6} f_i(k\delta x,L_y) - f_i(k\delta x,0) + \sum_{i=4,7,8} f_i(k\delta x,\delta x) - f_i(k\delta x,L_y+\delta x)\right] \quad (11)$$

to vanish separately. We therefore use Φ_y as a second control variable.

To control j_y^{tot}, we use the density difference $\Delta\rho_y$ as the actuating variable. Similarly, the reference density at the lower boundary ρ_B is used as the actuating variable controlling the net leakage Φ_y. Both actuating variables are adjusted using a standard PD controller algorithm [22], such that

$$-\frac{d}{dt}\Delta\rho_y = K_d\frac{d}{dt}j_y^{\mathrm{tot}} + K_p j_y^{\mathrm{tot}} \quad (12)$$

and accordingly for ρ_B and Φ_y. We refer to these boundary conditions in the following as adaptive generalized periodic boundary conditions (AGPBC).

III. SIMULATION RESULTS

In order to be able to evaluate the precision of our proposed boundary conditions, a control system needs to be defined. We will take this control system from a reference system that includes several unit cells in y-direction as well as the confining walls. The effects of the walls on the flow are hence fully captured, although finite size effects limiting the periodicity may arise.

Consider an extended array of unit cells as shown in Fig. 1. Using GPBC (whose accuracy was tested against a Poiseuille flow in [12]) in x direction, this array can be reduced to a $1\cdot M_y$ array. A unit cell grid of $N_x=N_y=200$ lattice nodes is used. Each unit cell contains a solid triangular obstacle. We choose $M_y=7$, which is enough to achieve sufficient periodicity at the inner cells and can still be easily simulated with modern computers. The LBM relaxation time is set to $\tau=0.8$, corresponding to a kinematic viscosity of $\nu=\delta x^2/10\delta t$. Using the resulting average flow velocity and the horizontal length of the obstacle as characteristic length and velocity, this setup corresponds to a Reynolds number of $R\approx 10^{-1}$. This is an approximate upper boundary for our method since above this threshold, time dependencies—albeit very small ones—make it impossible to compare the accuracy in the stationary case at the achieved level. Furthermore, existing microfluidic devices typically work significantly below this threshold, e.g., [13] with $R\approx 10^{-4}$.

The value of $\Delta\rho_y$ was adjusted using $K_d=0.8\times10^{-5}$, $K_p=0.8\times10^{-6}$ (ρ_B: $K_d=0.5\times10^{-5}$, $K_p=0.5\times10^{-4}$). Initially, the fluid in the system is inert. The simulation is run for 400,000 steps. The controller loop was started after an initialization period of $\Delta t^{\mathrm{init}}=10\,000\delta t$, to avoid initial effects affecting the control variables. In the following, we use the central unit cell of this array as our control system. Density averages at $x=0$ and $x=L_x+\delta x$ are set to 1.000 01 and 1.0, respectively. This leads to small deviations in the control system. Because of the proximity of upper and lower walls, the flow velocities over the top and bottom most cells and the inner cells differ. Since the average density difference $\Delta\rho_x$ over the entire array (i.e., averaging from $y=\delta x$ to $y=M_y\cdot L_y$) is kept fixed, this leads to an effective density gradient over the control system different from that over the single cells. This error, however, is a finite size effect intrinsic to the control system and is not related to the single cells' setup. It would vanish if the number of outer cells became negligible compared to the number of inner cells.

In what follows, we use the control system to test the accuracy of a single unit cell using AGPBC. For comparison, we also show the results for a cell that uses simple GPBC in x but SPBC in y direction, ignoring the effects of an asymmetric obstacle.

The resulting flow isolines $|\mathbf{v}|$ after 300 000 simulation steps are shown in Fig. 2. Figure 2(a) shows the results for AGPBC, while Fig. 2(b) gives the isolines for GPBC. In both parts, the isolines of the control system are depicted as thicker gray lines. Results for AGPBC coincide with the control system to a degree where the isolines become indistinguishable. In contrast, deviations are clearly visible for GPBC, where deviations in the velocity are of the same order of magnitude as the average flow velocity.

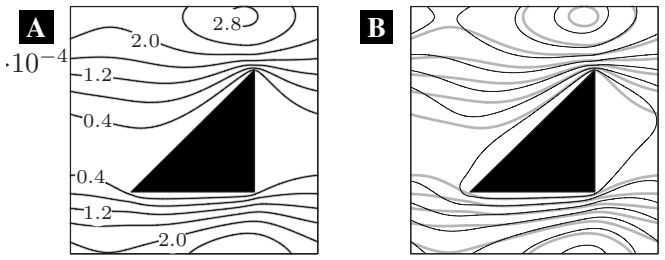

FIG. 2. Flow isolines ($|\mathbf{v}|$) of the control system (thick gray lines) and the single cells (thin black lines) for AGPBC (a) and simple GPBC (b). Velocity isolines are spaced $4\times10^{-5}\delta x/\delta t$. All values are given in units of 10^{-4}, as indicated by the prefactor on the left of the figure.

To quantify these deviations, we compute the deviations against the flow velocity of the control system $\mathbf{v}_{\mathrm{ctrl}}$ relative to the mean-square flow velocity $\overline{\mathbf{v}}^2_{\mathrm{ctrl}}$ as

$$\epsilon = \sqrt{\frac{(\mathbf{v}_{\mathrm{ctrl}}-\mathbf{v})^2}{\overline{\mathbf{v}}^2_{\mathrm{ctrl}}}} \tag{13}$$

Deviations are shown in Fig. 3. Figure 3(a) shows the deviations between the control system and the system with AGPBC. The errors are of the order of 10^{-4}. In particular, the error in the velocity appears to be proportional to the velocity itself, indicating that it may stem from the small difference in the effective $\Delta\rho_x$ discussed above. In addition, this difference is of the same order as the observed error $(\Delta\rho_x^{\mathrm{AGPBC}}-\Delta\rho_x^{\mathrm{ctrl}})/\Delta\rho_x\approx10^{-4}$. To test this hypothesis, we simulate the AGPBC system and apply the effective $\Delta\rho_x$ of the control system. Results for identical effective pressure are shown in part B. The error is reduced by several orders of magnitude, showing that the originally observed error was caused by the mismatch in $\Delta\rho_x$. Furthermore, such an error is of a particular type, since only the flow velocity but not the flow pattern is altered. In fact, a simple rescaling of the flow velocities in order to re-match the density gradients would suffice to reduce the error by the same order of magnitude (data not shown). At the same time, the error for a system using simple GPBC would be of order 10^{-1}.

The time evolution of the adaptive density gradient is shown in Fig. 4. After the initialization period, a very short period with strong fluctuations follows. However, these fluctuations are quickly suppressed. Compared with the density

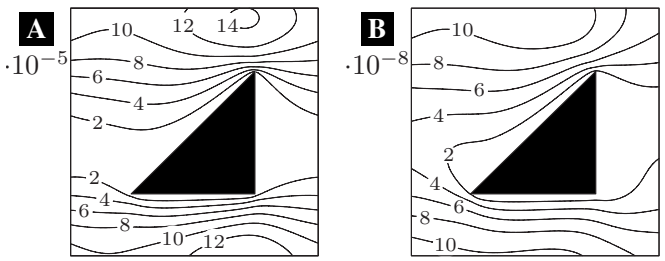

FIG. 3. Relative deviations ϵ between the control system and the adaptive system with original $\Delta\rho_x$ (a) and with the control system's effective $\Delta\rho_x$ (b). Values are given in units of the prefactor, printed on the left of each figure.

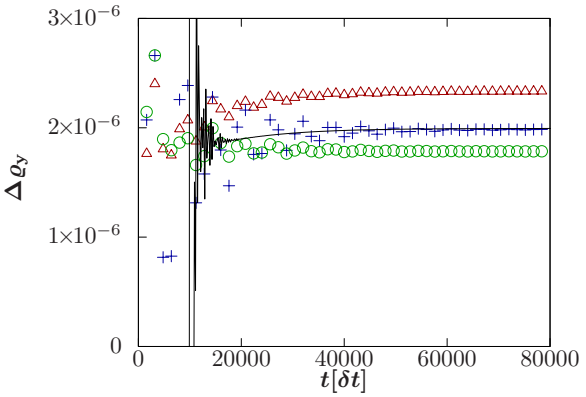

FIG. 4. (Color online) Evolution of the adaptive density gradient (solid line) compared to the density difference over the topmost (green circles), central (blue crosses) and bottommost (red triangles) unit cells of the control array.

gradient over the control system, the adaptive density gradient thereafter converges faster and with smaller fluctuations against its long time limit. Notably, the density difference over the outermost cells differs significantly. This is caused by the presence of the solid outer walls which slow down the flow considerably. However, already for our seven-cell system, such deviations occur only for the cells in direct contact with the solid walls. Density differences over all unit cells are shown in Fig. 5 for the long time limit when numerical accuracy was reached ($t\approx4\times10^5\delta t$). The differences over all inner cells are virtually identical and agree very well with the resulting $\Delta\varrho_y$ over the AGPBC unit cell.

Figure 6 shows the approach to the long time limit for the absolute currents $|j_y^{\mathrm{tot}}|$ (Panel B), the absolute leakage $|\Phi_y|$ (Panel C), and their control quantities $\Delta\rho_y$ and ρ_B. Both control quantities show a regular exponential decay with a time constant of $\lambda\approx-1/12\,000\delta t$. For comparison, panel A shows the decay of the vertical flow through the lower control cell boundary $j_\perp^{\mathrm{ctrl}}(y=600\delta x)$, and the approach of the corresponding density difference between the upper and lower boundary of the control cell $\Delta\rho_y^{\mathrm{ctrl}}$ to its long time value.

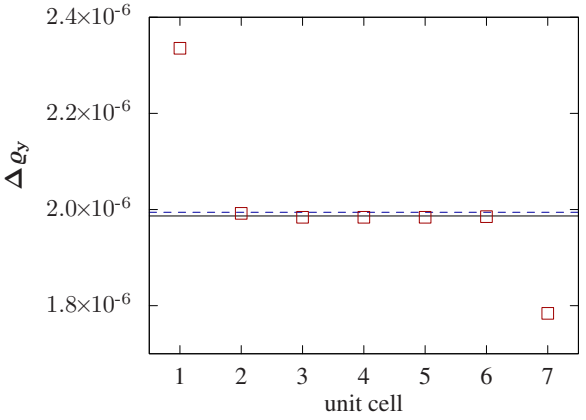

FIG. 5. (Color online) Long-time limit values of the density difference over different unit cells of the control array (red squares), with the applied adaptive difference $\Delta\rho_y$ (dashed blue line, between nodes 0 and 201) and the resulting periodic difference $\Delta\varrho_y$ (solid black line, between nodes 1 and 201) as horizontal lines.

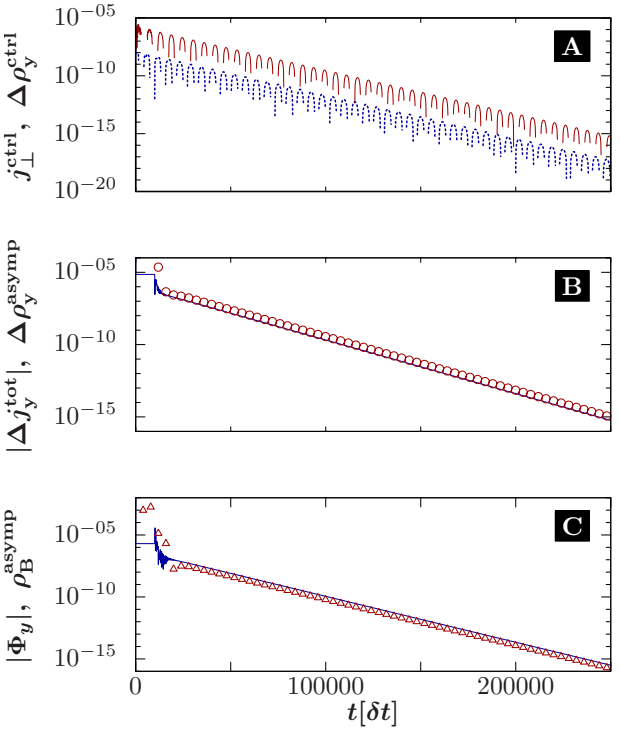

FIG. 6. (Color online) Panel A: Decay of the net flow $j_\perp^{\mathrm{ctrl}}(y=600\delta x)$ through a horizontal boundary (red line) and of the corresponding asymptotic density difference $\Delta\rho_y^{\mathrm{ctrl}}=\Delta\rho_y^{\mathrm{ctrl}}(t)-\Delta\rho_y^{\mathrm{ctrl}}(\infty)$ measured over the control cell, i.e., between lines $y=600$ and $y=800$ of the array (blue dotted line). Since the quantities decay oscillatory, no absolute value was taken and hence only the positive parts are displayed. Panel B: Relaxation of absolute total y momentum $|j_y^{\mathrm{tot}}|$ (red circles) and controlling density difference $\Delta\rho_y^{\mathrm{asymp}}=|\Delta\rho_y(t)-\Delta\rho_y(\infty)|$ (blue line) in the AGPBC system. Panel C: Relaxation of absolute leakage $|\Phi_y|$ (red triangles) and the controlling average bottom density $\rho_B^{\mathrm{asymp}}=|\rho_B(t)-\rho_B(\infty)|$ (blue line) in the AGPBC system.

Although the decay of these quantities is oscillatory, the decay constant is virtually identical to the AGPBC system, demonstrating that both our initial condition Eq. (5) and our implementation method are valid. Within the simulated time interval, all control quantities have reached numerical accuracy and are significantly below the mean observed error. Compared to the control system, the AGPBC system is able to obtain virtually identical accuracy within the same time. For implementation purposes it should be noted that the long time decay depends largely on the geometry of the simulated system, and on whether the flow is increasing or decaying to a long time limit. The latter is a significantly slower process that can occur if the adaptive pressure gradient forces the flow into a direction where it experiences a much larger resistance. It can be avoided through a suitable choice of controller coefficients, appropriate initialization times, or a gradual onset of the driving density gradient [22].

IV. CONCLUSION

We proposed a boundary condition for the treatment of periodic structures confined by solid walls in lattice-Boltzmann simulations. Within a single unit cell, the effect of the walls is simulated by an adaptive pressure gradient. The velocities calculated with our method are in agreement with the reference system. Using these boundary conditions, it is possible to fully exploit periodicity in both dimensions. Therefore, the size of the system can be reduced to a single unit cell, leading to decreased simulation times or increased spatial resolution. Hence, microfluidic devices, which use various forms of unit cell layouts, can be efficiently simulated using the lattice-Boltzmann method. In particular, the calculation of flows in microfluidic devices with large numbers of unit cells benefits from our proposed boundary condition. A good example for such a device is the deterministic lateral displacement array for continuous particle separation [13]. For this class of devices, the computational effort can be reduced significantly.

ACKNOWLEDGMENTS

One of us (O.G.) acknowledges travel support during the course of this work provided by the Department of Physics at the Chinese University of Hong Kong. We also would like to thank Pak-Ming Hui for helpful discussions and comments on an earlier draft of this manuscript.

[1] S. Chen and G. Doolen, Annu. Rev. Fluid Mech. **30**, 329 (1998).
[2] S. Succi, *The Lattice Boltzmann Equation for Fluid Dynamics and Beyond* (Oxford University Press, New York, 2001).
[3] M. C. Sukop and D. T. J. Thorne, *Lattice Boltzmann Modeling: An Introduction for Geoscientists and Engineers* (Springer, Berlin, Germany, 2007).
[4] P. Lavallée, J. P. Boon, and A. Noullez, Physica D **47**, 233 (1991).
[5] Q. Zou and X. He, Phys. Fluids **9**, 1591 (1997).
[6] I. Ginzburg and D. d'Humières, Phys. Rev. E **68**, 066614 (2003).
[7] S. Ansumali and I. V. Karlin, Phys. Rev. E **66**, 026311 (2002).
[8] J. Latt, B. Chopard, O. Malaspinas, M. Deville, and A. Michler, Phys. Rev. E **77**, 056703 (2008).
[9] Z. Yuan, W. Tao, and Q. Wang, Int. J. Numer. Methods Fluids **28**, 1371 (1998).
[10] D. Kandhai, A. Koponen, A. Hoekstra, and M. Kataja, J. Comput. Phys. **150**, 482 (1999).
[11] J. Zhang and D. Y. Kwok, Phys. Rev. E **73**, 047702 (2006).
[12] S. Kim and H. Pitsch, Phys. Fluids **19**, 108101 (2007).
[13] L. Huang, E. Cox, R. Austin, and J. Sturm, Science **304**, 987 (2004).
[14] D. Inglis, Appl. Phys. Lett. **94**, 013510 (2009).
[15] Z. Li and G. Drazer, Phys. Rev. Lett. **98**, 050602 (2007).
[16] A. De Leebeeck, L. K. S. Kumar, V. de Lange, D. Sinton, R.

Gordon, and A. G. Brolo, Anal. Chem. **79**, 4094 (2007).
[17] A. Stroock, S. Dertinger, G. Whitesides, and A. Ajdari, Anal. Chem. **74**, 5306 (2002).
[18] As commonly done in the discussion of LBM, all quantities are in the following given in units of δx, δt, and combinations thereof.
[19] P. Bhatnagar, E. Gross, and M. Krook, Phys. Rev. **94**, 511 (1954).
[20] Y. H. Qian and Y. Zhou, Phys. Rev. E **61**, 2103 (2000).
[21] T. Krüger, F. Varnik, and D. Raabe, Phys. Rev. E **79**, 046704 (2009).
[22] R. C. Dorf and R. H. Bishop, *Modern Control Systems* (Prentice Hall, Englewood Cliffs, NJ, 2008).